

CYBER AIDD

WEEKLY REPORT



CyberAIDD assisted analysis of drug discovery article Titled “Discovery of Potent Orally Bioavailable Tricyclic NLRP3 Inhibitor”

(Reference: J.Med.Chem.2024,67,2,1544-1562)

Part-1

NLRP3 is a molecular sensor that recognizes a variety of red flags. Activation of NLRP3 can induce the assembly of inflammasomes, which activates caspase-1, followed by the maturation of the pro-inflammatory cytokines IL-1 β and IL-18, as well as Gasdermin-D cleavage and pyroptosis cell death. NLRP3 inflammasomes have been linked to a variety of diseases, including gout, type 2 diabetes, atherosclerosis, Alzheimer's disease, and cancer. This article describes a novel tricyclic NLRP3 backbone discovered by high-throughput screening. Hit 1 was optimized to obtain the first-arrival compound NP3-562, which showed excellent potency in human whole blood and completely inhibited IL-1 β release in a mouse model of acute peritonitis at an oral dose of 30 mg/kg. Compared to known sulfonylurea inhibitors, the X-ray structure of NP3-562 binding to the NLRP3 NAHT domain reveals a unique binding pattern.

Here efforts are made to provide insights on how Pharmacodia's CyberSAR platform can play a key role in improving efficiency of study, providing an in-depth elucidation of NLRP3 inhibitor molecules. The system shows the active molecules associated with the target through the cluster structure view and the original structure view, and presents the potential Hit in the form of a timeline of the R&D stage. In addition, CyberSAR also provides visual analysis of indications and trial design, helping developers quickly obtain target structure information and develop research ideas. Although CyberSAR has not been used in the initial development of molecules, it has shown great potential for application in the elucidation and optimization of drug molecules.

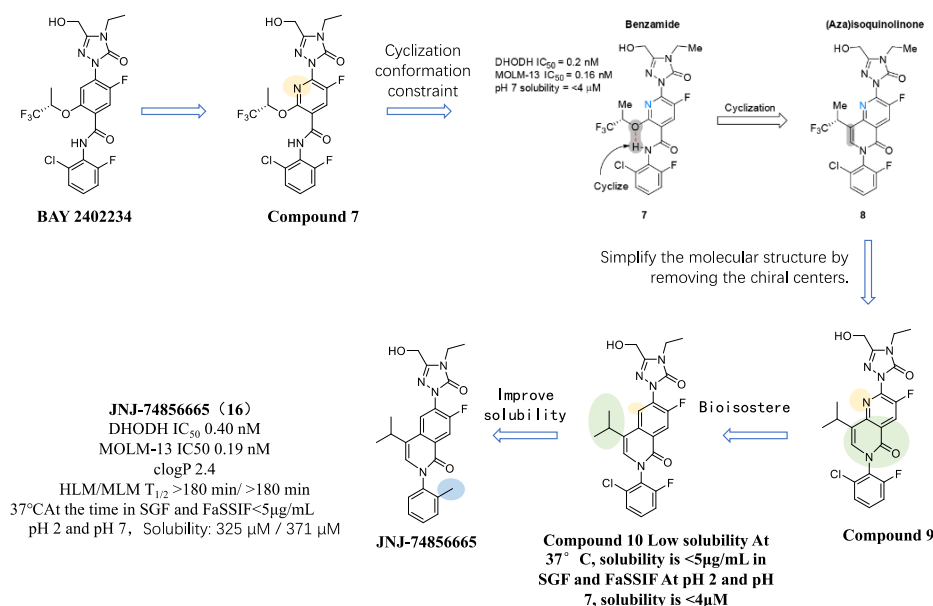
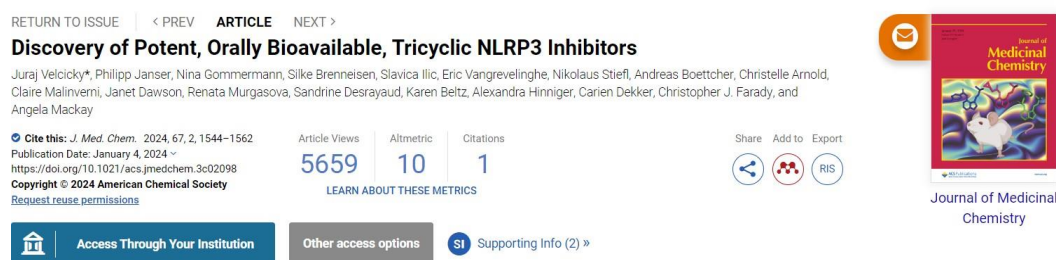


Figure 1. NP3–562 discovery and molecular optimization process



The innate immune system plays a key role in tissue homeostasis and host defense against invading microorganisms. However, its aberrant activation may lead to widespread autoinflammatory and autoimmune diseases. When exposed to pathogens, tissue-resident cells (including epithelial cells, macrophages, dendritic cells) respond quickly to destroy pathogens by releasing antimicrobial peptides or phagocytosis. In addition, they secrete cytokines and chemokines that recruit monocytes and neutrophils to the site of infection, leading to inflammation and local tissue damage. Innate immune cells recognize common microbial-specific molecules, such as viral nucleic acids or bacterial lipopolysaccharides (LPS), mannose, or flagellates, through pattern recognition receptors (PRRs). In addition to pathogen-associated molecular patterns (PAMPs), some PRRs can detect damage-associated molecular patterns (DAPs), sterile exogenous danger signals, or molecules released from damaged or dying cells, including ATP, and uric acid crystals or amyloid β protein ($A\beta$). NLRP3, also known as cryopyrin, is an intracellular PRR consisting of 3 domains: an N-terminal pyrin domain, a central nucleotide-binding domain (NACHT), and a leucine-rich repeating domain. Cytosolic NLRP3 acts as a sensor to recognize PAMP and DAMP-induced stress signals, and upon activation, oligomerizes and recruits ASCs (apoptosis-associated dot-like proteins containing the caspase recruitment domain) and procaspase-1 to form macromolecular inflammasome complexes. This complex allows proximity-based procaspase-1 to be automatically activated and subsequently cleaved with pro-IL-1 β as well as pro-IL-18 and Gasdermin-D.

The pro-inflammatory cytokines IL-1 β and IL-18 have been shown to play a role in a variety of diseases. IL-1 neutralization is a key therapeutic pathway for rare autoinflammatory diseases, including cold pyriine-associated periodic syndrome (CAPS), which is caused by gain-of-function mutations in NLRP3. In addition, IL-1 β has been shown to play an important role in chronic diseases such as gout or type 2 diabetes, as well as neuroinflammatory diseases, including multiple sclerosis, Alzheimer's disease, or diabetic neuropathy. In addition, the CANTOS study is a study of secondary risk prevention of cardiovascular disease using IL-1 β monoclonal antibodies, and canakinumab has shown that IL-1 β causes cardiovascular risk, lung cancer, and osteoarthritis. NLRP3, as the primary inflammasome sensor for sterile

danger signals associated with many of these diseases, has emerged as a potential druggable therapeutic target for small molecule drug discovery, with the potential to inhibit IL-1 β , IL-18, and pyroptosis, and to penetrate tissues where biologics cannot act. MCC950 (also known as CP-456 or CRID3) acts as a true NLRP3 inhibitor with biochemical and crystallography demonstrating direct binding to the NLRP3 NACHT domain. The first wave of MCC950-derived NLRP3 inhibitors such as ZYIL1, GDC-2394, and NT-0796 (Figure 1) entered early clinical development. These compounds have safety concerns, such as hepatotoxicity. There is a need to explore more chemical space and develop safe and potent NLRP3 inhibitors to maximize development. In this paper, the authors describe a novel potent and orally available tricyclic NLRP3 inhibitor.

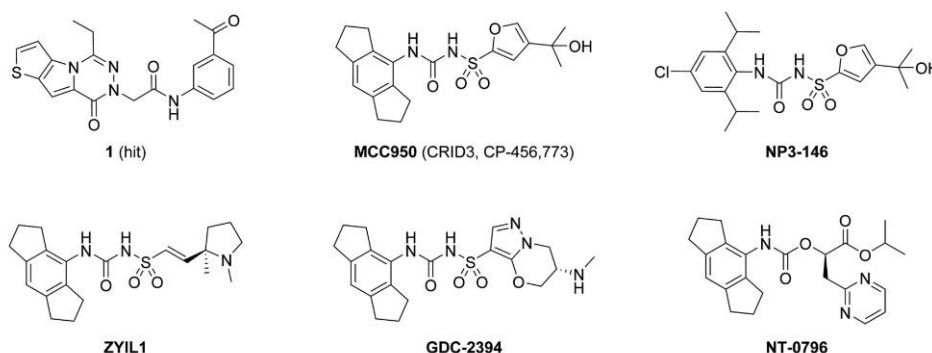
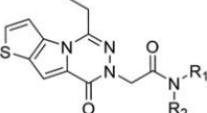


Figure 1. Structures of hit 1 and selected NLRP3 inhibitors.

To identify novel NLRP3 inhibitors, i.e., backbones with different structural and physicochemical properties from known sulfonylurea-based NLRP3 binders, a high-throughput screening of Novartis' in-house compound libraries was conducted. The pyroptosis protection of PMA-differentiated THP-1 cells was induced by nigericin as a method for primary screening, which could distinguish between cytotoxic compounds, and pyroptosis was also the result of three different types of NLRP3 inflammasome activation pathways known to be caused, and the hit rate of primary screening was very low. Subsequent screening used nigericin-induced inhibition of IL-1 β secretion in THP-1 cells and TNF- α secretion in Pam3CSK4-stimulated THP-1 cells, which together can mimic the NLRP3 inflammasome classical activation pathway. In addition, the binding of compounds to the MCC950 binding pocket in the NLRP3 protein was analyzed using a recombinant NLRP3 NACHT domain and a fluorescently labeled sulfonylurea probe of NP3-14624 (Figure 1) using the previously described biochemical fluorescence polarization (FP) assay. Several hits were screened, of which compound 1 from a commercial library (Figure 1) was used as the initiating hit compound because it had a relatively potent inhibitory effect on the release of IL-1 β from nigericin-stimulated THP-1 cells (0.63 μ M, Table 1). Compound 1 was shown to bind directly to NLRP3 in the biochemical FP assay (IC₅₀ of 1.13 μ M) and did not inhibit the release of TNF- α in THP-1 cells (IC₅₀ >100 μ M).

Table 1. Optimization of the Amide Substituent in the Hit 1

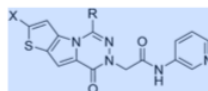


| Compd. | R ₁ | R ₂ | IL-1 β THP-1 ^a [μ M] | HT Eq. solubility ^b [mM] | MDCK LE ^c Papp A-B [10 ⁻⁶ cm/s] | Clint ^d HLM [μ L/min/mg] |
|--------|----------------|----------------|--|---|---|---|
| 1 | | H | 0.625 \pm 0.024 | 0.004 | 41 | 299 |
| 2 | | H | 0.330 \pm 0.044 | 0.002 | 25 | 269 |
| 3 | Me | H | 2.62 \pm 1.13 | 0.128 | 26 | 54 |
| 4 | | Me | 82 \pm 2 | 0.006 | 19 | 971 |
| 5 | | H | 0.250 \pm 0.051 | 0.021 | 27 | 63 |
| 6 | | H | 0.104 \pm 0.012 | 0.007 | 21 | 69 |
| 7 | | H | 0.043 \pm 0.002 | 0.004 | 5.7 | 405 |
| 8 | | H | 1.15 \pm 0.17 | >1.0 | 0.7 | <10 |

^aIC₅₀ determined as a mean \pm SEM ($n \geq 2$) in homogeneous time resolved fluorescence (HTRF) assay measuring IL-1 β levels in the supernatant of nigericin-stimulated THP-1 cells. ^bHigh-throughput equilibrium solubility determined by saturation shake flask method³⁷ at pH 6.8 using DMSO solution. ^cPermeability coefficient apical-basolateral (P_{app} A-B) determined in a high-throughput low efflux Madin-Darby canine kidney cells (MDCK) assay.³⁶ ^dIntrinsic clearance determined by the disappearance of the parent compound from the reaction media using human liver microsomes.

SAR exploration begins with derivatization of amide substituents using commercially available acid 22 (Table 1). Initial SAR using the IL-1 β inhibitory activity assay in THP-1 cells showed a slight increase in acetyl2 potency on aniline removed from compound 1 (0.33 μ M, Table 1). The removal of amide aryl ring 3 resulted in a nearly 10-fold loss of potency compared to compound 2, indicating the need for a larger substituent at this location. In addition, the amide represented by N-Me analogue 4 lost its activity (82 μ M), indicating that amide-NH is necessary for binding NLRP3. Due to the lack of crystal structure data, it is unclear whether the presence of tertiary amides has a detrimental effect. Integration of nitrogen functional groups into aromatic rings, such as 3-pyridyl derivatives 5, did not affect potency, but improved solubility and intrinsic clearance of liver microsomes (Table 1). The addition of one more nitrogen atom, such as pyrimidine derivative 6, was improved (104 nM) activity, but the solubility was reduced. Interestingly, the hydroxyl group at aniline 3 such as Chem7 further increased the potency (43 nM), suggesting that the hydrogen donor at this position may be beneficial for binding to NLRP3. However, all other properties are degraded compared to pyridine analogues 5 (Table 1). In general, almost all early compounds exhibit poor water solubility. To improve solubility, Novartis tries to reduce the planar signature of the molecule by increasing the carbon bond saturation (sp^3 fraction). Partial saturation of the tricyclic system, e.g. changing thiophene to cyclopentene ring (data not shown), does not increase solubility, so the amination of 3-piperidinamide 8 with an aromatic group is improved (>1 mM), most likely due to the presence of base nitrogen. In addition, it has higher metabolic stability in humans (<10 μ L/min/mg, Table 1) as well as in mouse and rat liver microsomes (50 and 40 μ L/min/mg, data not shown) compared to other analogues in this series. However, the permeability of 8 measured in the low-throughput Madin-Darby canine kidney cell (MDCK LE) assay is very low (less than 1×10^{-6} cm/s, Table 1), most likely due to its high hydrophilicity (log D_{7.4} of -0.2). Therefore, Novartis retains the 3-pyridyl substituent for further optimization because of its good potency and good overall characteristics.

Table 2. Optimization of the Tricycle

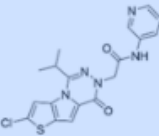
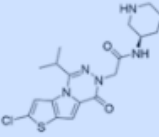
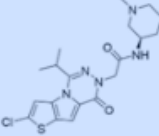
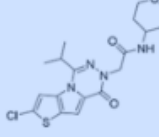
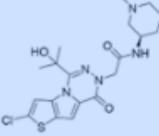
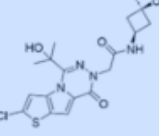
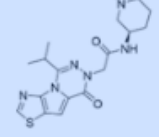


| Compd. | X | R | IL-1 β THP-1 ^a [μ M] | IL-1 β whole blood ^b [μ M] | HT Eq. solubility ^c [mM] | logD _{7.4} | Clint ^d HLM/MLM [μ L/min/mg] |
|--------|----|--------------|--|--|---|---------------------|--|
| 5 | H | Et | 0.250 \pm 0.051 | 3.76 \pm 1.91 | 0.021 | 2.6 | 63 / 412 |
| 9 | H | H | 1.90 \pm 0.61 | 7.28 \pm 5.09 | 0.091 | 1.9 | <10 / 48 |
| 10 | H | <i>n</i> -Pr | 1.72 \pm 0.18 | 15.9 \pm 6.1 | 0.003 | 3.0 | 101 / >1000 |
| 11 | H | <i>i</i> -Pr | 0.069 \pm 0.005 | 1.98 \pm 0.91 | 0.019 | 3.1 | 144 / 490 |
| 12 | H | | 0.115 \pm 0.021 | 3.14 \pm 1.23 | 0.026 | 2.7 | 76 / 464 |
| 13 | H | | 0.086 \pm 0.010 | 1.13 \pm 0.05 | 0.023 | 2.8 | 68 / 300 |
| 14 | F | <i>i</i> -Pr | 0.227 \pm 0.017 | 8.80 \pm 7.54 | 0.251 | 3.4 | 79 / 227 |
| 15 | Cl | <i>i</i> -Pr | 0.143 \pm 0.029 | 9.75 \pm 1.12 | 0.010 | 4.0 | 44 / 124 |

^aIC₅₀ determined as a mean \pm SEM ($n \geq 2$) in HTRF assay measuring IL-1 β levels in the supernatant of nigericin-stimulated THP-1 cells. ^bIC₅₀ determined as a mean \pm SEM ($n \geq 2$) in IL-1 β release from LPS/ATP stimulated human whole blood. ^cHigh-throughput equilibrium solubility determined by saturation shake flask method³⁷ at pH 6.8 using DMSO solution. ^dIntrinsic clearance determined by the disappearance of the parent compound from the reaction media using human (HLM) and mouse liver microsomes (MLM).

For skeleton optimization, Novartis turned its attention to the three rings (Table 2). The removal of ethyl groups such as Compound 9 (1.90 μ M) is significantly less potent than Compound 5 (0.25 μ M), indicating that this substituent is important for binding to NLRP3. On the other hand, compound 9 exhibited good solubility and clearance (Table 2), probably due to its reduced lipophilicity (0.7 logarithmic units lower). In addition to the increased solubility (91vs21 μ M), the metabolic stability of compound 9 was significantly improved compared to ethyl-substituted 5. Ethyl substituents, similar to N- PR10, also resulted in decreased cellular potency (1.72 μ M, Table 2). In this case, the reduced potency may be due to the limited space in this protein region, and the efficacy of the isopropyl derivative 11 is significantly increased (IC₅₀ 0.069 μ M, Table 2). The lipophilicity of the two compounds 10 and 11 is increased and their metabolic stability is reduced. Cyclopropyl 12 and alcohol derivatives 13 help to reduce lipophilicity and clearance, at least similar to compound 11 in HLM, while maintaining potency. Since there was no significant improvement in metabolic stability, Novartis further investigated specific sites of metabolism. To do this, compound 11 was incubated with human liver microsomes and analyzed for biotransformation using liquid chromatography tandem mass spectrometry (LC-MS/MS). Interestingly, P450-driven thiophene epoxidation was identified as the major metabolite. Thiophenol oxidation is a well-documented biotransformation, and the oxidation of thiophene carbon atoms is thought to form epoxides. Thiophene epoxide stands for reactive electrophile and reacts with a variety of nucleophiles that can cause toxicity. To explore the formation of such reactive metabolites, compound 11 was incubated with human liver microsomes with NADPH and glutathione (GSH) as trapping agents, confirming the formation of GSH adducts. Interestingly, a more polar and metabolically stable derivative 13 was also observed to form GSH adducts. Metabolism in vivo decreases after thiophene 2-position. Thus, the formation of reactive intermediates of 2-fluoro- and 2-chloro- analogues (compounds 14 and 15) of 11 was tested, and the formation of GSH adducts was not observed for either compound. While both compounds lost some potency, chlorine analogue 15 was more metabolically stable (Table 2).

Table 3- Property Optimization of 15

| Compd. | Structure | IL-1 β THP-1 ^a [μ M] | IL-1 β whole blood ^b [μ M] | HT Eq. solubility ^c [mM] | logD _{7.4} | Clint ^d HLM/MLM [μ L/min/mg] | CL mouse ^e [mL/min/kg] | F/ [%] | AUCinf po ^f [nmol.h/L] |
|---------------|---|--|--|---|---------------------|--|--------------------------------------|---------------|--------------------------------------|
| 15 |  | 0.143 \pm 0.029 | 9.75 \pm 1.12 | 0.010 | 4.0 | 44 / 124 | 16.5 \pm 0.8 | 55 \pm 18 | 3748 \pm NA |
| 16 |  | 0.107 \pm 0.023 | 1.02 \pm 0.03 | >1.0 | 1.0 | 12 / 55 | 55.7 \pm 10.2 | 27.6 \pm NA | 691 \pm NA |
| 17 |  | 0.084 \pm 0.013 | 0.701 \pm 0.200 | >1.0 | 2.4 | 59 / 364 | 58 \pm 10.6 | 7.8 \pm 2.4 | 163 \pm 44 |
| 18 |  | 0.165 \pm 0.025 | 3.04 \pm 1.00 | 0.003 | 3.0 | 30 / 129 | NA | NA | NA |
| 19 NP3-562 |  | 0.090 \pm 0.051 | 0.214 \pm 0.084 | >1.0 | 2.3 | 38 / 103 | 58 \pm NA | 36 \pm 8 | 718 \pm 165 |
| 20 |  | 0.006 \pm 0.003 | 0.093 \pm 0.039 | 0.036 | 2.8 | <10 / 33 | NA | NA | NA |
| 21 |  | 0.068 \pm 0.001 | 0.500 \pm 0.007 | >1.0 | 1.1 | 27 / 231 | NA | NA | NA |

^aIC₅₀ determined as a mean \pm SEM ($n \geq 2$) in HTRF assay measuring IL-1 β levels in the supernatant of nigericin-stimulated THP-1 cells. ^bIC₅₀ determined as a mean \pm SEM ($n \geq 2$) in 50% human whole blood measuring IL-1 β levels after LPS/ATP stimulation. ^cHigh-throughput equilibrium solubility determined by saturation shake flask method³⁷ at pH 6.8 using DMSO solution. ^dIntrinsic clearance determined by the disappearance of the parent compound from the reaction media using human liver microsomes (HLM) and mouse liver microsomes (MLM). ^eClearance measured as a mean \pm SD of 4 animals (male C57BL/6) after iv dosing (1 mg/kg) using NMP/Plasma (10:90) formulation. ^fOral bioavailability \pm SD calculated as dose-normalized ratio of AUCextrap po to AUCextrap iv, both parameters determined as a mean \pm SD of 3 animals (male C57BL/6). ^gOral exposure measured as a mean \pm SD of 3 animals (male C57BL/6) after po dosing (3 mg/kg) using MC/Water/Tween (0.5:99.4:0.1) formulation. SD only provided if the elimination phase was fully characterized for all 3 animals. NA = not available.

Compound 15 has high lipophilicity (log $D_{7.4}$ of 4.0), poor solubility (10 μM), and low potency in human whole blood (9.75 μM), so further modification of the skeleton is required (Table 3). Inspired by analogues 8 (Table 1), piperidine analogues 16 modulate lipophilicity and solubility, and as expected, both parameters of 16 were significantly improved while cellular potency was maintained (Table 3). Importantly, a large increase in polarity (1.0 log $D_{7.4}$) and its potency in human whole blood (1.02 μM compared to 9.75 μM for 15, Table 3). However, the theoretical exposure of compound 16 was significantly reduced in mice (Table 3), possibly due to its reduced permeability (3×10^{-6} cm/s). In addition, compound 16 showed cardiac risk because of inhibition of human hERG with an IC_{50} of 26 μM . Interestingly, its N-Me-analogue 17 exhibits lower hERG inhibition ($\text{IC}_{50} > 30 \mu\text{M}$) while increasing potency in THP-1 cells and whole blood. Surprisingly, despite the good permeability of compound 17 (15×10^{-6} cm/s), its bioavailability and oral exposure in mice are very low. By substituting the amine with another ether substituent, 18, the intrinsic clearance of compound 17 can be improved. However, the potency and solubility of this compound are below 17 (Table 3). Metabolic stability can also be improved by combining NMe-piperidine substituents with alcohol-containing tricyclic compounds 19 (NP3-562). Although in vivo clearance in mice was still comparable to 17 (Table 3), there was a significant improvement in bioavailability and oral exposure. What's more, the compound exhibited excellent potency in whole blood, so its in vivo inhibitory effect on IL-1 β was tested. To this end, an acute LPS/ATP-driven peritonitis model was used to examine the pharmacokinetic/pharmacodynamic (PK/PD) relationship of NLRP3 inhibitors. The compound is orally administered to female C57BL/6 mice 1 h prior to peritoneal (i.p.) injection of LPS. ATP activates NLRP3 inflammasome after 2 h injection, and peritoneal IL-1 β levels and blood compound concentrations are measured 15 min after ATP triggering. NP3-562 showed robust, dose-dependent inhibition of IL-1 β in this model (Figure 2), with greater than 90% inhibition at 100 and 30 mg/kg doses, while underdose proportional exposure and reduced efficacy were observed at 10 mg/kg doses. In vitro, the IC_{50} of IL-1 β secretion in the whole blood of 50% mice stimulated with LPS/ATP is 248 nM, which correlates with the observed 45% inhibited blood concentration (163 nM) at 10 mg/kg. Similarly, 91% inhibition was observed at a blood exposure of 1059 nM (30 mg/kg), compared to the calculated IC_{90} ($10 \times \text{IC}_{50}$) for the mouse whole blood assay) is fairly consistent, indicating a good correlation between in vitro whole blood assays and in vivo cytokine inhibition in this model (Figure 2). In separate experiments, NP3-562 at a dose of 50 mg/kg resulted in 90% IL-1 inhibition at blood concentrations of $1.68 \pm 0.53 \mu\text{M}$. In this experiment, the brain exposure of the compound was determined to be $0.398 \pm 0.147 \mu\text{M}$, thus demonstrating that NP3-562 can act on the central nervous system ($\text{Kp } 0.2$).

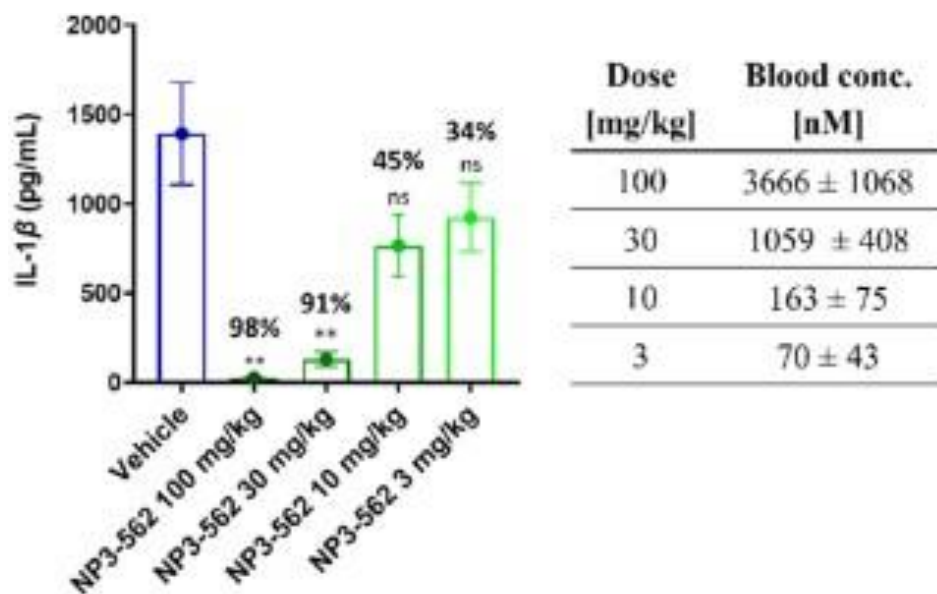


Figure 2. NP3–562 (19) was orally dosed to female C57BL/6 mice 1 h before an intraperitoneal injection of LPS followed by ATP injection 2 h later. 15 min after ATP stimulation, animals were sacrificed, the peritoneum was washed with PBS, and IL-1 β was measured in peritoneal lavage. Data are presented as mean \pm SD (n = 5 mice/group); ** p < 0.01, n.s.: not significant, ordinary one-way ANOVA followed by Dunnett’s multiple comparisons test vs LPS/vehicle-treated mice.

To further increase potency, additional substitution of piperidine substituents was explored, and the discovery of alcohol derivatives²⁰ demonstrated that the backbone has very high cellular potency (6 nM, Table 3). As associated with phenol 7 (Table 1), this result indicates the binding of the hydrogen bond donor to NLRP3 in this region. However, this substituent reduced solubility, and 20 showed a slight increase in potency in whole blood compared to NP3–562 (Table 3). The use of thiazole instead of 2-chlorothiophene yields a more polar derivative 21 (log $D_{7.4}$ of 1.1) with potency results comparable to those of its compounds in cells and whole blood (Table 3). However, both compounds (20 and 21) exhibit only moderate protection against IL-1 β release in the peritonitis model (30% and 40% for 20 or 2, respectively), which is consistent with low blood exposure (65 nM for 20 and 113 nM for 21) after 50 mg/kg oral dose of aldose sugar.

Overall, NP3–562 exhibited good overall characteristics. The thermodynamic solubility of the crystal form obtained by crystallization from hot butanone was measured 6.8 at pH of 159 mg/L. In addition, ithadaclean off-target features include no mutagenic results, no interference with the NFκB pathway (TNFα IC₅₀ >100 μM), hERG inhibition measured at 30 μM and IC₅₀ >25 μM for the 3A4, 2D6, and 2C9 cytochrome P450 isoforms. NP3–562 was tested in a broader set of enzymes, receptors, and channels, showing good selectivity for more than 90 off-targets tested at 10 μM concentrations, although it showed some inhibition of VMAT-2, IC₅₀ is 6.5 μM. The biotransformation of NP3–562 in rat, canine and human liver microsomes mainly occurs around the piperidine ring, with N-demethylation as the main metabolite. More importantly, thiophene oxidation and no GSH adduct formation were observed in none of the three species after NP3–562 biological activation. In vitro clearance was measured in mouse, rat, canine, and human liver microsomes of 103, 100, 39, and 37 μL/min/mg, respectively, and plasma protein binding rates of 97%, 78%, 83%, and 85% for these species, respectively. The PK profile of NP3–562 measured in three different species (mouse, rat, and dog) showed comparable clearance between the different species, approximately 40% of the hepatic blood flow in a single species. However, more favorable half-lives and improved oral bioavailability were observed in rats and dogs compared to mice (Table 4).

Table 4. Pharmacokinetic Profile of NP3-562 in Different Species

| species | mouse | rat | dog |
|-----------------------|----------|-----------|------------|
| dose (iv/po, mg/kg) | 1/3 | 1/10 | 0.1/1 |
| CL [mL/min/kg] | 85 ± NA | 34 ± 11 | 12.4 ± 4.5 |
| V _m [L/kg] | 3.9 ± NA | 5.5 ± 1.8 | 4.1 ± 1.2 |
| t _{1/2} [h] | 1.0 ± NA | 3.5 ± 3.2 | 5.7 ± 0.5 |
| AUC po dn [nmol·h/L] | 235 ± 56 | 712 ± 249 | 2530 ± 239 |
| F [%] | 36 ± 8 | 63 ± 22 | 89 ± 25 |

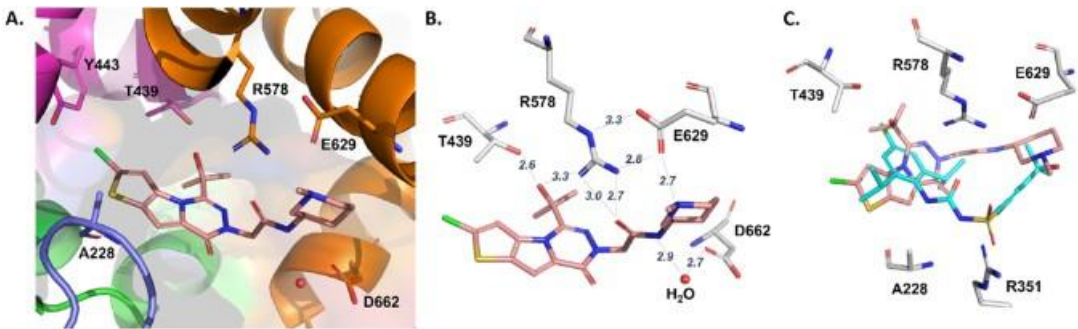


Figure 3. A. NP3–562 (pink) bound to the NACHT domain binding site (PDB: 8RI2). The subdomains of the NACHT domain are colored as follows: NBD, purple; HD1, green; WHD, magenta; HD2, orange. B. Polar interactions of NP3–562 and the protein are indicated by dotted lines with the distance in Angstrom shown. C. Overlay of NP3–562 (pink) and NP3–146²⁴ (PDB: 7ALV, cyan) bound to NACHT domain binding site.

In the FP binding assay, the IC₅₀ of NP3-562 was 0.26 μ M, indicating that the compound binds to the same ligand binding site in the NACHT domain of NLRP3 as the MCC950 analogue. This was confirmed by the co-crystallization of NP3-562 with the NLRP3 NACHT domain (Fig. 3). The crystal structure (PDB:8RI2) was resolved to 2.8Å resolution, showing a clear density of NP3-562 at known ligand binding sites. As shown in Figure 3A, the ligand binding site is located at the interface of four subdomains of the NACHT domain – nucleotide binding domain (NBD), helical domain 1 (HD1), wing helix domain (WHD), and helical domain 2 (HD2). The crystal structure shows that the tricyclic binding of NP3-562 to a hydrophobic pocket formed by several amino acids containing lipophilic residues. The key polar interactions are formed by the adaptor amide carbonyl group and Arg578 residue of the ligand (Figure 3B). While coordinating with Glu629, Arg578 also interacts with the triazine ring of NP3-562 amide cation. In addition, Arg578 makes a third contact with the ligand by interacting with alcohol substituents, which are also involved in the interaction with Thr439. Another important ligand-protein interaction is mediated by the anionic interaction of Glu629 residues with piperidine nitrogen in NP3-562. The 2.8Å resolution allows the placement of several water molecules, one of which was found to be involved in the water-mediated interaction between the amide-NH and Asp662 residues of the ligand, which illustrates the importance of the ligand secondary amide. In the published NLRP3 structure complexed with NP3-146 (PDB:7ALV), the backbone carbonyl group of Ala228 provides a critical interaction with the ligand, but NP3-562 does not observe this interaction. In addition, there was no polar interaction between NP3-562 and Walker A motif of NLRP3. Comparison of the binding mode of NP3-562 to NLRP3 with that of NP3-146 shows that NP3-562 also does not interact with Arg351, while this amino acid residue is involved in the interaction with NP3-146. Thus, NP3-562 and NP3-146 bind to the same pocket, but the tricyclic and sulfonylurea series have unique pharmacophores and occupy this site in different ways (Figure 3C).

Conclusion

In this paper, Novartis discloses the discovery and optimization of a novel NLRP3 binding backbone. Hit compound 1 was identified by high-throughput screening of THP-1 cells. Through the exploration of its amide function and tricyclic compounds, SAR was established. The initial compounds, especially tea aniline analogues, are less water-soluble. Due to the presence of base nitrogen and the increase in SP³ hybridization fraction, the solubility can be improved by using piperidine-substituted amides. The thiophene ring needs to be substituted to avoid bioactivation and the formation of GSH adducts, and the 2-chloride substitution on thiophene has good potency and metabolic stability. Finally, the compound NP3-562 was discovered. Its binding to NLRP3 can be confirmed by the X-ray crystal structure of NP3-562 binding to the NACHT domain at 2.8Å resolution. NP3-562 binds to the same pocket as the previously discovered sulfonylurea scaffold (NP3-146), but has a different binding pattern than NP3-146 because it occupies a slightly different space in the pocket of the NACHT domain. In addition, the importance of several substituents of this backbone for binding to the pocket, such as the lipophilic/aromatic nature of the tricyclic group, the linking amide (carbonyl oxygen and NH), the piperidine ring (including its positive charge), and the hydroxyl group on the tricyclic thanks to its interaction with Tyr439, allowing polarity to be added to another lipophilic pocket. With the exception of strong efficacy in the acute peritonitis model (91% at 30 mg/kg), it did not exhibit significant

inhibition of major off-target (including hERG, CYP, and enzyme and receptor panels). In addition, it does not show any inducing potential, nor does GSH adducts show any inducing potential. The combination of good in vitro and in vivo ADME properties and good potency in human blood (0.21 μM) demonstrates the potential for further development of this backbone, laying the groundwork for the development of analogues for further study of NLRP3 biology.

Part II

Reference: <https://doi.org/10.1021/acs.jmedchem.3c02098>

Part III

1. Combined with drug design ideas, Pharmacodia CyberSAR excavates the active structure reported in the literature and patents, and uses CyberSAR to quickly obtain the target structure of interest of R&D personnel for developing ideas, and NLRP3 (Homo sapiens) is given as an example:

The screenshot displays the Pharmacodia CyberSAR web application interface. The top navigation bar includes 'Home', 'CyberX-SAR', 'CyberX-Discovery', 'CyberX-Virtual Library', and 'Customized Services'. A search bar is set to 'Target' with 'NLRP3' entered. A dropdown menu shows search results for 'NLRP3', including 'NLRP3 (NACHT, LRR and PYD domains-containing protein 3 | Homo sapiens)', 'NLRP3 (NACHT, LRR and PYD domains-containing protein 3 | Mus musculus)', 'Nlrp3/Pycard (Nlrp3/Pycard | Mus musculus)', 'NLRP3-NEK7 (NLRP3-NEK7 | Mus musculus)', and 'NLRP1 (NACHT, LRR and PYD domains-containing protein 1 | Homo sapiens)'. Below the search bar, three main sections are visible: 'CyberX-SAR' (Known SAR map), 'CyberX-Discovery' (AI-driven drug discovery toolkit), and 'CyberX-Virtual Library' (Real-based virtual compound libraries). Each section contains icons, descriptions, and buttons for further actions like 'Target Overview', 'Chemical Space', 'AI Computation', and 'GPCR Library'.

2. The PDB code of the eutectic structure of "NLRP3 (Homo sapiens)" and the corresponding ligand small molecule structure are included in the target interface, which can efficiently and conveniently obtain the ligand small molecule structure and interaction mode in the eutectic structure of the target.

Home > Target Overview > Target Detail

NLRP3 : NACHT, LRR and PYD domains-containing protein 3 (Homo sapiens)

Structure Info

Indication

ChemSpace

Assay Data

Bioassay

SAR Doc

Target Landscape

Name And Taxonomy

| | |
|-------------------------------|---|
| Name | NACHT, LRR and PYD domains-containing protein 3 |
| Synonyms | NLR Family Pyrin Domain Containing 3 AGTAVPRL Deafness, Autosomal Dominant 34 PYRIN-containing APAF1-like protein 1 NLR Family, Pyrin Domain-Containing 3 Protein NACHT Domain-, Leucine-Rich Repeat-, And PYD-Containing Protein 3 Caterpillar protein 1.1 Cryopyrin, NACHT, LRR And PYD Domains - Containing Protein 3 NACHT, LRR And PYD Domains-Containing Protein 3 FCAS ... |
| Organism | Homo sapiens |
| Class | - Unclassified protein |
| Type | SINGLE PROTEIN |
| Ext. Links | GenCards OpenTarget UniProt PDB AlphaFold |
| Physiological Function | Sensor component of the NLRP3 inflammasome, which mediates inflammasome activation in response to defects in membrane integrity, leading to secretion of... |

Components

3D Structure

With Ligands

6WSM (PDB) 8SKN (PDB) 8SWK (PDB) 8ETR (PDB) 8EJ4 (PDB) 7VTP (PDB) 7PZC (PDB) 7ALV (PDB)

Others

6WSM With Ligands (1)

XE3 (Preclinical)

Ligands

6 Results

8GI (Preclinical)

Co-crystal Targets: NLRP3

AGS (Preclinical)

Co-crystal Targets: SYN1 BST1 F261 ...

RM5 (Preclinical)

Co-crystal Targets: NLRP3

WTN (Preclinical)

Co-crystal Targets: NLRP3

XE3 (Preclinical)

Co-crystal Targets: NLRP3

1 2

3. Select the cascade "Cluster Structure View" tab under the "Chemical Space" option tab in the target interface, and the literature and patents included in the CyberSAR platform can display the molecules with experimental test activity related to NLRP3 (Homo sapiens) in the form of "parent nuclear structure clustering". Among them, the "highlighted" in green font is the active molecular structure of IC₅₀ <1000 nM in the in vitro enzyme and cell activity test experiments reported in the literature, the specific experiment, the experimental results and the experimental source.

NLRP3 : NACHT, LRR and PYD domains-containing protein 3 (Homo sapiens)

Structure Info

Indication

ChemSpace

Assay Data

Bioassay

SAR Doc

Target Landscape

Real Structure

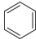

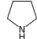
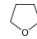
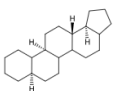
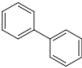
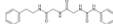
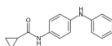
Cluster Structure (100)

Clustering Threshold

Loose

Strict

Tips: 1- The chemical space includes molecules labeled manually and those identified through experimental data mining; 2- Manual labels are sourced from the Pharmacodia global drug database and other manually confirmed sources; Active molecules are those with activity indicators $\leq 1000\text{nM}$; 3- The R&D status reflects the highest development status of the molecules contained in the cluster.

| | | | |
|--|--|--|--|
| <div>CC266528</div> <div></div> <div> <div>Clustered Mol: 26838</div> <div>Active Mol: 6</div> <div>Clinical Mol: 637 (Approved)</div> </div> | <div>CC332024</div> <div></div> <div> <div>Clustered Mol: 1907</div> <div>Active Mol: 1</div> <div>Clinical Mol: 57 (Approved)</div> </div> | <div>CC332275</div> <div></div> <div> <div>Clustered Mol: 3376</div> <div>Active Mol: 0</div> <div>Clinical Mol: 53 (Approved)</div> </div> | <div>CC642850</div> <div></div> <div> <div>Clustered Mol: 1191</div> <div>Active Mol: 0</div> <div>Clinical Mol: 48 (Approved)</div> </div> |
| <div>CC643412</div> <div></div> | <div>CC642974</div> <div></div> | <div>CC642693</div> <div></div> | <div>CC642744</div> <div></div> |

4. Select the cascading "Real Structure View" tab under the "Chemical Space" option tab in the target interface, and the molecules with NLRP3 (Homo sapiens) related experimental test activity in the literature included in the CyberSAR platform can be displayed in the form of "R&D stage timeline". Among them, "data mining" highlighted in green font is potential Hit

The screenshot shows the "NLRP3 : NACHT, LRR and PYD domains-containing protein 3 (Homo sapiens)" target overview. The interface includes a sidebar with navigation options like "Structure Info", "Indication", "ChemSpace", "Assay Data", "Bioassay", and "SAR Doc". The main content area displays a timeline of molecules categorized by their R&D stage:

- Approved (3):** Sulopenem etzdroxil..., Berdazimer sodium, Sodium taurodeoxyc...
- Phase 3 Clinical (2):** Nitrozetone, Dapansutrile
- Phase 2 Clinical (2):** Usnoflast, Vodudeutentan
- Phase 1 Clinical (5):** Inzomelid, BMS-986299, Selnoflast, Luxeptinib
- Preclinical (419):** (Multiple molecules shown)

Each molecule entry includes its chemical structure, name, and a "Data Mining" status. A "Click to View Molecule Details" button is also present.

To Explore Cyber-AIDD further Login on your computer using the below Link

<https://cyber.pharmacodia.com/#/homePage>

If you need further assistance contact us,

For a free trial, Contact us on

Anil Ranadev
+91 9742627845
anil_ranadev@saspinjara.com

Aravind P
+91 9619076286
aravind.p@saspinjara.com

Sachin Marihal
+91 9538033363
sachin.marihal@saspinjara.com

Chetan S
+91 7022031061
chetans@saspinjara.com

